SUPPLEMENTARY INFORMATION

doi:10.1038/nature14422

1 Methods

Notations

- **c**: Parameters of a controller (vector)
- **x**: A location in a discrete behavioral space (i.e. a type of behavior) (vector)
- χ: A location in a discrete behavioral space that has been tested on the physical robot (vector)
- $\mathscr{P}$: Behavior-performance map (stores performance) (associative table)
- $\mathscr{C}$: Behavior-performance map (stores controllers) (associative table)
- $\mathscr{P}(\mathbf{x})$: Max performance yet encountered at **x** (scalar)
- $\mathscr{C}(\mathbf{x})$: Controller currently stored in **x** (vector)
- $\chi_{\mathbf{1:t}}$: All previously tested behavioral descriptors at time t (vector of vectors)
- $\mathbf{P_{1:t}}$: Performance in reality of all the candidate solutions tested on the robot up to time t (vector)
- $\mathscr{P}(\chi_{\mathbf{1:t}})$: Performance in the behavior-performance map for all the candidate solutions tested on the robot up to time t (vector)
- $f()$: Performance function (unknown by the algorithm) (function)
- σ^2_{noise}: Observation noise (a user-specified parameter) (scalar)
- $k(\mathbf{x},\mathbf{x})$: Kernel function (see section "kernel function") (function)
- **K**: Kernel matrix (matrix)
- **k**: Kernel vector $[k(\mathbf{x},\chi_1), k(\mathbf{x},\chi_2), ..., k(\mathbf{x},\chi_t)]$ (vector)
- $\mu_t(\mathbf{x})$: Predicted performance for **x** (i.e. the mean of the Gaussian process) (function)
- $\sigma^2_t(\mathbf{x})$: Standard deviation for **x** in the Gaussian process (function)

1.1 Intelligent Trial and Error algorithm (IT&E)

The Intelligent Trial and Error Algorithm consists of two major steps (Extended Data Fig. 1): the behavior-performance map creation step and the adaptation step (while here we focus on damage recovery, Intelligent Trial and Error can search for any type of required adaptation, such as learning an initial gait for an undamaged robot, adapting to new environments, etc.). The behavior-performance map creation step is accomplished via a new algorithm introduced in this paper called multi-dimensional archive of phenotypic elites (MAP-Elites), which is explained in the next section. The adaptation step is accomplished via a second new algorithm introduced in this paper called the map-based Bayesian optimization algorithm (M-BOA), which is explained in the "Adaptation Step" section below.

1.2 Behavior-performance map creation (via the MAP-Elites algorithm)

The behavior-performance map is created by a new algorithm we introduce in this paper called the multi-dimensional archive of phenotypic elites (MAP-Elites) algorithm. MAP-Elites searches for the highest-performing solution for each point in a user-defined space: the user chooses the dimensions of the space that they are interested in seeing variation in. For example, when designing robots, the user may be interested in seeing the highest-performing solution at each point in a two-dimensional space where one axis is the weight of the robot and the other axis is the height of the robot. Alternatively, a user may wish to see weight vs. cost, or see solutions throughout a 3D space of weight vs. cost vs. height. Any dimension that can vary could be chosen by the user. There is no limit on the number of dimensions that can be chosen, although it becomes computationally more expensive to fill the behavior-performance map and store it as the number of dimensions increases. It also becomes more difficult to visualize the results. We refer to this user-defined space as the "behavior space", because usually the dimensions of variation measure behavioral characteristics. Note that the behavioral space can refer to other aspects of the solution (as in this example, where the dimensions of variation are physical properties of a robot such as its height and weight).

If the behavior descriptors and the parameters of the controller are the same (i.e. if there is only one possible solution/genome/parameter set/policy/description for each location in the behavioral space), then creating the behavior-performance map is straightforward: one simply needs to simulate the solution at each location in the behavior space and record the performance. However, if it is not known a priori how to produce a controller/parameter set/description that will end up in a specific location in the behavior space (i.e. if the parameter space is of higher dimension than the behavioral space: e.g., in our example, if there are many different robot designs of a specific weight, height, and cost, or if it is unknown how to make a description that will produce a robot with a specific weight, height, and cost), then MAP-Elites is beneficial. It will efficiently search for the highest-performing solution at each point of the low-dimensional behavioral space. It is more efficient than a random sampling of the search space because high-performing solutions are often similar in many ways, such that randomly altering a high-performing solution of one type can produce a high-performing solution of a different type (see Supplementary Fig. 3 and Supplementary Experiment S4). For this reason, searching for high-performing solutions of all types simultaneously is much quicker than separately searching for each type. For example, to generate a lightweight, high-performing robot design, it tends to be more effective and efficient to modify an existing design of a light robot rather than randomly generate new designs from scratch or launch a separate search process for each new type of design.

MAP-Elites begins by generating a set of random candidate solutions. It then evaluates the performance of each solution and records where that solution is located in the behavior space (e.g. if the dimensions of the behavior space are the height and weight, it records the height and weight of each robot in addition to its performance). For each solution, if its performance is better than the current solution at that location in the behavior-performance map, then it is added to the behavior-performance map, replacing the solution in that location. In other words, it is only kept if it is the best of that type of solution, where "type" is defined as a location in the behavior space. There is thus only one solution kept at each location in the behavior space (keeping more could be beneficial, but for computational reasons we only keep one). If no solution is present in the behavior-performance map at that location, then the newly generated candidate solution is added at that location.

Once this initialization step is finished, Map-Elites enters a loop that is similar to stochastic, population-based, optimization algorithms, such as evolutionary algorithms[1]: the solutions that are in the behavior-performance map form a population that is improved by random variation and selection. In each generation, the algorithm picks a solution at random via a uniform distribution, meaning that each solution has an equal chance of being chosen. A copy of the selected solution is then randomly mutated to change it in some way, its performance is evaluated, its location in the behavioral space is determined, and it is kept if it outperforms the current occupant at that point in the behavior space (note that mutated solutions may end up in different behavior space locations than their "parents"). This process is repeated until a stopping criterion is met (e.g. after a fixed

amount of time has expired). In our experiments, we stopped each MAP-Elites run after 40 million iterations. Because MAP-Elites is a stochastic search process, each resultant behavior-performance map can be different, both in terms of the number of locations in the behavioral space for which a candidate is found, and in terms of the performance of the candidate in each location.

The pseudo-code of the algorithm is available in Supplementary Figure 1. More details and experiments about MAP-Elites are available in (Mouret and Clune, 2015)[2].

1.3 Adaptation step (via M-BOA: the map-based Bayesian optimization algorithm)

The adaptation step is accomplished via a Bayesian optimization algorithm seeded with a behavior-performance map. We call this approach a map-based Bayesian optimization algorithm, or M-BOA.

Bayesian optimization is a model-based, black-box optimization algorithm that is tailored for very expensive objective functions (a.k.a. cost functions)[3, 4, 5, 6, 7, 8]. As a black-box optimization algorithm, Bayesian optimization searches for the maximum of an unknown objective function from which samples can be obtained (e.g., by measuring the performance of a robot). Like all model-based optimization algorithms (e.g. surrogate-based algorithms[9, 10, 11], kriging[12], or DACE[13, 14]), Bayesian optimization creates a model of the objective function with a regression method, uses this model to select the next point to acquire, then updates the model, etc. It is called *Bayesian* because, in its general formulation[5], this algorithm chooses the next point by computing a posterior distribution of the objective function using the likelihood of the data already acquired and a prior on the type of function.

Here we use Gaussian process regression to find a model[15], which is a common choice for Bayesian optimization[16, 7, 4, 3]. Gaussian processes are particularly interesting for regression because they not only model the cost function, but also the uncertainty associated with each prediction. For a cost function f, usually unknown, a Gaussian process defines the probability distribution of the possible values $f(\mathbf{x})$ for each point $\mathbf{x}$. These probability distributions are Gaussian, and are therefore defined by a mean (μ) and a standard deviation (σ). However, μ and σ can be different for each $\mathbf{x}$; we therefore define a probability distribution *over functions*:

$$P(f(\mathbf{x})|\mathbf{x}) = \mathcal{N}(\mu(\mathbf{x}), \sigma^2(\mathbf{x})) \tag{1}$$

where $\mathcal{N}$ denotes the standard normal distribution.

To estimate $\mu(\mathbf{x})$ and $\sigma(\mathbf{x})$, we need to fit the Gaussian process to the data. To do so, we assume that each observation $f(\chi)$ is a sample from a normal distribution. If we have a data set made of several observations, that is, $f(\chi_1), f(\chi_2), ..., f(\chi_t)$, then the vector $[f(\chi_1), f(\chi_2), ..., f(\chi_t)]$ is a sample from a *multivariate* normal distribution, which is defined by a mean vector and a covariance matrix. A Gaussian process is therefore a generalization of a n-variate normal distribution, where n is the number of observations. The covariance matrix is what relates one observation to another: two observations that correspond to nearby values of χ_1 and χ_2 are likely to be correlated (this is a prior assumption based on the fact that functions tend to be smooth, and is injected into the algorithm via a prior on the likelihood of functions), two observations that correspond to distant values of χ_1 and χ_2 should not influence each other (i.e. their distributions are not correlated). Put differently, the covariance matrix represents that distant samples are almost uncorrelated and nearby samples are strongly correlated. This covariance matrix is defined via a *kernel function*, called $k(\chi_1, \chi_2)$, which is usually based on the Euclidean distance between χ_1 and χ_2 (see the "kernel function" subsection below).

Given a set of observations $\mathbf{P}_{1:t} = f(\chi_{1:t})$ and a sampling noise σ^2_{noise}(which is a user-specified parameter), the Gaussian process is computed as follows[4, 15]:

$$\begin{aligned} &P(f(\mathbf{x})|\mathbf{P}_{1:t}, \mathbf{x}) = \mathcal{N}(\mu_t(\mathbf{x}), \sigma^2_t(\mathbf{x})) \\ &\text{where :} \\ &\mu_t(\mathbf{x}) = \mathbf{k}^\top \mathbf{K}^{-1} \mathbf{P}_{1:t} \\ &\sigma^2_t(\mathbf{x}) = k(\mathbf{x}, \mathbf{x}) - \mathbf{k}^\top \mathbf{K}^{-1} \mathbf{k} \\ &\mathbf{K} = \begin{bmatrix} k(\chi_1, \chi_1) & \cdots & k(\chi_1, \chi_t) \\ \vdots & \ddots & \vdots \\ k(\chi_t, \chi_1) & \cdots & k(\chi_t, \chi_t) \end{bmatrix} + \sigma^2_{noise} I \\ &\mathbf{k} = \begin{bmatrix} k(\mathbf{x}, \chi_1) & k(\mathbf{x}, \chi_2) & \cdots & k(\mathbf{x}, \chi_t) \end{bmatrix} \end{aligned} \tag{2}$$

Our implementation of Bayesian optimization uses this Gaussian process model to search for the maximum of the objective function $f(\mathbf{x})$, $f(\mathbf{x})$ being unknown. It selects the next χ to test by selecting the maximum of the *acquisition function*, which balances exploration – improving the model in the less explored parts of the search space – and exploitation – favoring parts that the models predicts as promising. Here, we use the "Upper Confidence Bound" acquisition function (see the "information acquisition function" section below). Once the observation is made, the algorithm updates the Gaussian process to take the new data into account. In classic Bayesian optimization, the Gaussian process is initialized with a constant mean because it is assumed that all the points of the search space are equally likely to be good. The model is then progressively refined after each observation.

The key concept of the map-based Bayesian optimization algorithm (M-BOA) is to use the output of MAP-Elites as a prior for the Bayesian optimization algorithm: thanks to the simulations, we expect some behaviors to perform better than others on the robot. To incorporate this idea into the Bayesian optimization, M-BOA models the *difference* between the prediction of the behavior-performance map and the actual performance on the real robot, instead of directly modeling the objective function. This idea is incorporated into the Gaussian process by modifying the update equation for the mean function ($\mu_t(\mathbf{x})$, equation 2):

$$\mu_t(\mathbf{x}) = \mathscr{P}(\mathbf{x}) + \mathbf{k}^\top \mathbf{K}^{-1} (\mathbf{P}_{1:t} - \mathscr{P}(\chi_{1:t})) \tag{3}$$

where $\mathscr{P}(\mathbf{x})$ is the performance of $\mathbf{x}$ according to the simulation and $\mathscr{P}(\chi_{1:t})$ is the performance of all the previous observations, also according to the simulation. Replacing $\mathbf{P}_{1:t}$ (eq. 2) by $\mathbf{P}_{1:t} - \mathscr{P}(\chi_{1:t})$ (eq. 3) means that the Gaussian process models the difference between the actual performance $\mathbf{P}_{1:t}$ and the performance from the behavior-performance map $\mathscr{P}(\chi_{1:t})$. The term $\mathscr{P}(\mathbf{x})$ is the prediction of the behavior-performance map. M-BOA therefore starts with the prediction from the behavior-performance map and corrects it with the Gaussian process.

The pseudo-code of the algorithm is available in Supplementary Figure 1.

Kernel function The kernel function is the covariance function of the Gaussian process. It defines the influence of a controller's performance (on the physical robot) on the performance and confidence estimations of not-yet-tested controllers in the behavior-performance

procedure INTELLIGENT TRIAL AND ERROR ALGORITHM (IT&E)
  Before the mission:
    CREATE BEHAVIOR-PERFORMANCE MAP (VIA THE MAP-ELITES ALGORITHM IN SIMULATION)
  while In mission **do**
    if Significant performance fall **then**
      ADAPTATION STEP (VIA M-BOA ALGORITHM)

procedure MAP-ELITES ALGORITHM
  $(\mathscr{P} \leftarrow \emptyset, \mathscr{C} \leftarrow \emptyset)$ ▷ *Creation of an empty behavior-performance map (empty N-dimensional grid).*
  for iter $= 1 \rightarrow I$ **do** ▷ *Repeat during I iterations (here we choose I = 40 million iterations).*
    if iter < 400 **then**
      $\mathbf{c}' \leftarrow$ random_controller() ▷ *The first 400 controllers are generated randomly.*
    else ▷ *The next controllers are generated using the map.*
      $\mathbf{c} \leftarrow$ random_selection$(\mathscr{C})$ ▷ *Randomly select a controller c in the map.*
      $\mathbf{c}' \leftarrow$ random_variation$(\mathbf{c})$ ▷ *Create a randomly modified copy of c.*
    $\mathbf{x}' \leftarrow$behavioral_descriptor(simu$(\mathbf{c}')$) ▷ *Simulate the controller and record its behavioral descriptor.*
    $p' \leftarrow$performance(simu$(\mathbf{c}')$) ▷ *Record its performance.*
    if $\mathscr{P}(\mathbf{x}') = \emptyset$ or $\mathscr{P}(\mathbf{x}') < p'$ **then** ▷ *If the cell is empty or if p' is better than the current stored performance.*
      $\mathscr{P}(\mathbf{x}') \leftarrow p'$ ▷ *Store the performance of $\mathbf{c}'$ in the behavior-performance map according to its behavioral descriptor $\mathbf{x}'$.*
      $\mathscr{C}(\mathbf{x}') \leftarrow \mathbf{c}'$ ▷ *Associate the controller with its behavioral descriptor.*
  return behavior-performance map ($\mathscr{P}$ and $\mathscr{C}$)

procedure M-BOA (MAP-BASED BAYESIAN OPTIMIZATION ALGORITHM)
  $\forall \mathbf{x} \in$ map: ▷ *Initialisation.*
    $P(f(\mathbf{x})|\mathbf{x}) = \mathcal{N}(\mu_0(\mathbf{x}), \sigma_0^2(\mathbf{x}))$ ▷ *Definition of the Gaussian Process.*
    where
    $\mu_0(\mathbf{x}) = \mathscr{P}(\mathbf{x})$ ▷ *Initialize the mean prior from the map.*
    $\sigma_0^2(\mathbf{x}) = k(\mathbf{x}, \mathbf{x})$ ▷ *Initialize the variance prior (in the common case, $k(\mathbf{x}, \mathbf{x}) = 1$).*
  while $\max(\mathbf{P_{1:t}}) < \alpha \max(\mu_t(\mathbf{x}))$ **do** ▷ *Iteration loop.*
    $\chi_{t+1} \leftarrow \arg\max_{\mathbf{x}}(\mu_t(\mathbf{x}) + \kappa\sigma_t(\mathbf{x}))$ ▷ *Select next test (argmax of acquisition function).*
    $P_{t+1} \leftarrow$ performance(physical_robot$(\mathscr{C}(\chi_{t+1}))$). ▷ *Evaluation of $\mathbf{x_{t+1}}$ on the physical robot.*
    $P(f(\mathbf{x})|\mathbf{P}_{1:t+1}, \mathbf{x}) = \mathcal{N}(\mu_{t+1}(\mathbf{x}), \sigma_{t+1}^2(\mathbf{x}))$ ▷ *Update the Gaussian Process.*
    where
    $\mu_{t+1}(\mathbf{x}) = \mathscr{P}(\mathbf{x}) + \mathbf{k}^\top \mathbf{K}^{-1}(\mathbf{P}_{1:t+1} - \mathscr{P}(\chi_{1:t+1}))$ ▷ *Update the mean.*
    $\sigma_{t+1}^2(\mathbf{x}) = k(\mathbf{x}, \mathbf{x}) - \mathbf{k}^\top \mathbf{K}^{-1} \mathbf{k}$ ▷ *Update the variance.*

$$\mathbf{K} = \begin{bmatrix} k(\chi_1, \chi_1) & \cdots & k(\chi_1, \chi_{t+1}) \\ \vdots & \ddots & \vdots \\ k(\chi_{t+1}, \chi_1) & \cdots & k(\chi_{t+1}, \chi_{t+1}) \end{bmatrix} + \sigma_{noise}^2 I$$ ▷ *Compute the observations' correlation matrix.*

$$\mathbf{k} = \begin{bmatrix} k(\mathbf{x}, \chi_1) & k(\mathbf{x}, \chi_2) & \cdots & k(\mathbf{x}, \chi_{t+1}) \end{bmatrix}$$ ▷ *Compute the $\mathbf{x}$ vs. observation correlation vector.*

Supplementary Figure 1 | Pseudo-code for the Intelligent Trial and Error Algorithm, the MAP-Elites algorithm, and the Map-based Bayesian Optimization Algorithm (M-BOA). Notations are described at the beginning of the methods section.

map that are nearby in behavior space to the tested controller (Supplementary Fig. 2a).

The Squared Exponential covariance function and the Matérn kernel are the most common kernels for Gaussian processes[4, 6, 15]. Both kernels are variants of the "bell curve". Here we chose the Matérn kernel because it is more general (it includes the Squared Exponential function as a special case) and because it allows us to control not only the distance at which effects become nearly zero (as a function of parameter ρ, Supplementary Fig. 2a), but also the rate at which distance effects decrease (as a function of parameter ν).

The Matérn kernel function is computed as follows[17, 18] (with $\nu = 5/2$):

$$k(\mathbf{x}_1, \mathbf{x}_2) = \left(1 + \frac{\sqrt{5}d(\mathbf{x}_1,\mathbf{x}_2)}{\rho} + \frac{5d(\mathbf{x}_1,\mathbf{x}_2)^2}{3\rho^2}\right)\exp\left(-\frac{\sqrt{5}d(\mathbf{x}_1,\mathbf{x}_2)}{\rho}\right) \quad (4)$$

where $d(\mathbf{x}_1, \mathbf{x}_2)$ is the Euclidean distance in behavior space.

Because the model update step directly depends on ρ, it is one of the most critical parameters of the Intelligent Trial and Error Algorithm. We selected its value after extensive experiments in simulation (Supplementary Fig. 2 and section 1.6).

Information acquisition function The information acquisition function selects the next solution that will be evaluated on the physical robot. The selection is made by finding the solution that maximizes the acquisition function. This step is another optimization problem, but does not require testing the controller in simulation or reality. In general, for this optimization problem we can derive the exact equation and find a solution with gradient-based optimization [19]. For the specific behavior space in the example problem in this paper, though, the discretized search space of the behavior-performance map is small enough that we can exhaustively compute the acquisition value of each solution of the behavior-performance map and then choose the maximum value.

Several different acquisition functions exist, such as the probability of improvement, the expected improvement, or the Upper Confidence Bound (UCB)[4, 16]. We chose UCB because it provided the best results in several previous studies[4, 16]. The equation for UCB is:

$$\mathbf{x}_{t+1} = \arg\max_{\mathbf{x}}(\mu_t(\mathbf{x}) + \kappa\sigma_t(\mathbf{x})) \quad (5)$$

where κ is a user-defined parameter that tunes the tradeoff between exploration and exploitation.

The acquisition function handles the exploitation/exploration trade-off of the adaptation (M-BOA) step. In the UCB function (Eq. 5), the emphasis on exploitation vs. exploration is explicit and easy to adjust. The UCB function can be seen as the maximum value (argmax) across all solutions of the weighted sum of the expected performance (mean of the Gaussian, $\mu_t(\mathbf{x})$) and of the uncertainty (standard deviation of the Gaussian, $\sigma_t(\mathbf{x})$) of each solution. This sum is weighted by the κ factor. With a low κ, the algorithm will choose solutions that are expected to be high-performing. Conversely, with a high κ, the algorithm will focus its search on unexplored areas of the search space that may have high-performing solutions. The κ factor enables fine adjustments to the exploitation/exploration trade-off of the M-BOA algorithm (the adaptation step). We describe how we chose the κ value in supplementary methods, section 1.6.

Code availability The source code (for GNU/Linux) for the experiments of this paper is available at the following URL:
`http://pages.isir.upmc.fr/~mouret/code/ite_source_code.tar.gz`

An implementation of the Bayesian optimization algorithm is freely available on:
`http://github.com/jbmouret/limbo`

1.4 Hexapod Experiment

Physical robot The robot is a 6-legged robot with 3 degrees of freedom (DOFs) per leg. Each DOF is actuated by position-controlled servos (MX-28 Dynamixel actuators manufactured by Robotis). The first servo controls the horizontal (front-back) orientation of the leg and the two others control its elevation. An RGB-D camera (Xtion, from ASUS) is fixed on top of the robot. Its data are used to estimate the forward displacement of the robot via an RGB-D SLAM algorithm* [20] from the robot operating system (ROS) framework† [21].

Simulator The simulator is a dynamic physics simulation of the undamaged 6-legged robot on flat ground (Fig. 4). We weighted each segment of the leg and the body of the real robot, and we used the same masses for the simulations. The simulator is based on the Open Dynamics Engine (ODE, `http://www.ode.org`).

Parametrized controller The angular position of each DOF is governed by a periodic function γ parametrized by its amplitude α, its phase ϕ, and its duty cycle τ (the duty cycle is the proportion of one period in which the joint is in its higher position). The function is defined with a square signal of frequency 1Hz, with amplitude α, and duty cycle τ. This signal is then smoothed via a Gaussian filter in order to remove sharp transitions, and is then shifted according to the phase ϕ.

Angular positions are sent to the servos every 30 ms. In order to keep the "tibia" of each leg vertical, the control signal of the third servo is the opposite of the second one. Consequently, angles sent to the i^{th} leg are:

- $\gamma(t, \alpha_{i_1}, \phi_{i_1}, \tau_{i_1})$ for DOF 1
- $\gamma(t, \alpha_{i_2}, \phi_{i_2}, \tau_{i_2})$ for DOF 2
- $-\gamma(t, \alpha_{i_2}, \phi_{i_2}, \tau_{i_2})$ for DOF 3

This controller makes the robot equivalent to a 12 DOF system, even though 18 motors are controlled.

There are 6 parameters for each leg $(\alpha_{i_1}, \alpha_{i_2}, \phi_{i_1}, \phi_{i_2}, \tau_{i_1}, \tau_{i_2})$, therefore each controller is fully described by 36 parameters. Each parameter can have one of these possible values: 0, 0.05, 0.1, ... 0.95, 1. Different values for these 36 parameters can produce numerous different gaits, from purely quadruped gaits to classic tripod gaits.

This controller is designed to be simple enough to show the performance of the algorithm in an intuitive setup. Nevertheless, the algorithm will work with any type of controller, including bio-inspired central pattern generators[22] and evolved neural networks[23, 24, 25, 26].

Reference controller Our reference controller is a classic tripod gait[27, 28, 29, 30, 31, 32]. It involves two tripods: legs 1-4-5 and legs 2-3-6 (Fig. 4). This controller is designed to always keep the robot balanced on at least one of these tripods. The walking gait is achieved by lifting one tripod, while the other tripod pushes the robot forward (by shifting itself backward). The lifted tripod is then placed forward in order to repeat the cycle with the other tripod. This gait is static, fast, and similar to insect gaits[28, 33].

*`http://wiki.ros.org/ccny_openni_launch`
†`http://www.ros.org`

Table S1 shows the 36 parameters of the reference controller. The amplitude orientation parameters (α_{i_1}) are set to 1 to produce the fastest possible gait, while the amplitude elevation parameters (α_{i_2}) are set to a small value (0.25) to keep the gait stable. The phase elevation parameters (ϕ_{i_2}) define two tripods: 0.25 for legs 2-3-5; 0.75 for legs 1-4-5. To achieve a cyclic motion of the leg, the phase orientation values (ϕ_{i_1}) are chosen by subtracting 0.25 to the phase elevation values (ϕ_{i_2}), plus a 0.5 shift for legs 1-3-5, which are on the left side of the robot. All the duty cycle parameters (τ_i) are set to 0.5 so that the motors spend the same proportion of time in their two limit angles. The actual speed of the reference controller is not important for the comparisons made in this paper: it is simply intended as a reference and to show that the performance of classic, hand-programmed gaits tend to fail when damage occurs.

Random variation of controller's parameters Each parameter of the controller has a 5% chance of being changed to any value in the set of possible values, with the new value chosen randomly from a uniform distribution over the possible values.

Main Behavioral descriptor (duty factor) The default behavioral descriptor is a 6-dimensional vector that corresponds to the proportion of time that each leg is in contact with the ground (also called duty factor). When a controller is simulated, the algorithm records at each time step (every 30 ms) whether each leg is in contact with the ground (1: contact, 0: no contact). The result is 6 Boolean time series (C_i for the i^{th} leg). The behavioral descriptor is then computed with the average of each time series:

$$\mathbf{x} = \begin{bmatrix} \frac{\sum_t C_1(t)}{\text{numTimesteps}(C_1)} \\ \vdots \\ \frac{\sum_t C_6(t)}{\text{numTimesteps}(C_6)} \end{bmatrix} \quad (6)$$

During the generation of the behavior-performance map, the behaviors are stored in the maps's cells by discretizing each dimension of the behavioral descriptor space with these five values: {0, 0.25, 0.5, 0.75, 1}. During the adaptation phase, the behavioral descriptors are used with their actual values and are thus not discretized.

Alternative Behavioral descriptor (orientation) The alternative behavioral descriptor tested on the physical robot (we investigated many other descriptors in simulation: Supplementary Experiment S5) characterizes changes in the angular position of the robot during walking, measured as the proportion of 15ms intervals that each of the pitch, roll and yaw angles of the robot frame are positive (three dimensions) and negative (three additional dimensions):

$$\mathbf{x} = \begin{bmatrix} \frac{1}{K}\sum_k U(\Theta^T(k) - 0.005\pi) \\ \frac{1}{K}\sum_k U(-\Theta^T(k) - 0.005\pi) \\ \frac{1}{K}\sum_k U(\Psi^T(k) - 0.005\pi) \\ \frac{1}{K}\sum_k U(-\Psi^T(k) - 0.005\pi) \\ \frac{1}{K}\sum_k U(\Phi^T(k) - 0.005\pi) \\ \frac{1}{K}\sum_k U(-\Phi^T(k) - 0.005\pi) \end{bmatrix} \quad (7)$$

where $\Theta^T(k)$, $\Psi^T(k)$ and $\Phi^T(k)$ denote the pitch, roll and yaw angles, respectively, of the robot torso (hence T) at the end of interval k, and K denotes the number of 15ms intervals during the 5 seconds of simulated movement (here, $K = 5s/0.015s \approx 334$). The unit step function $U(\cdot)$ returns 1 if its argument exceeds 0, and returns 0 otherwise. To discount for insignificant motion around 0 rad, orientation angles are only defined as positive if they exceed 0.5% of π rad. Similarly, orientation angles are only defined as negative if they are less than -0.5% of π rad.

Performance function In these experiments, the "mission" of the robot is to go forward as fast as possible. The performance of a controller, which is a set of parameters (section 1.4: Parametrized controller), is defined as how far the robot moves in a pre-specified direction in 5 seconds.

During the behavior-performance map creation step, the performance is obtained thanks to the simulation of the robot. All odometry results reported on the physical robot, during the adaptation step, are measured with the embedded simultaneous location and mapping (SLAM) algorithm[20]. The accuracy of this algorithm was evaluated by comparing its measurements to ones made by hand on 40 different walking gaits. These experiments revealed that the median measurement produced by the odometry algorithm is reasonably accurate, being just 2.2% lower than the handmade measurement (Supplementary Fig. 2d).

Some damage to the robot may make it flip over. In such cases, the visual odometry algorithm returns pathological distance-traveled measurements either several meters backward or forward. To remove these errors, we set all distance-traveled measurements less than zero or greater than two meters to zero. The result of this adjustment is that the algorithm appropriately considers such behaviors low-performing. Additionally, the SLAM algorithm sometimes reports substantially inaccurate low values (outliers on Supplementary Fig. 2d). In these cases the adaptation step algorithm will assume that the behavior is low-performing and will select another working behavior. Thus, the overall algorithm is not substantially impacted by such infrequent under-measurements of performance.

Stopping criterion In addition to guiding the learning process to the most promising area of the search space, the estimated performance of each solution in the map also informs the algorithm of the maximum performance that can be expected on the physical robot. For example, if there is no controller in the map that is expected to perform faster on the real robot than 0.3m/s, it is unlikely that a faster solution exists. This information is used in our algorithm to decide if it is worth continuing to search for a better controller; if the algorithm has already discovered a controller that performs nearly as well as the highest value predicted by the model, we can stop the search.

Formally, our stopping criterion is

$$\max(\mathbf{P}_{1:t}) \geq \alpha \max_{\mathbf{x} \in \mathscr{P}}(\mu_t(\mathbf{x})), \text{ with } \alpha = 0.9 \quad (8)$$

where $\mathbf{x}$ is a location in the discrete behavioral space (i.e. a type of behavior) and μ_t is the predicted performance of this type of behavior. Thus, when one of the tested solutions has a performance of 90% or higher of the maximum expected performance of any behavior in the map, the algorithm terminates. At that point, the highest-performing solution found so far will be the compensatory behavior that the algorithm selects. An alternative way the algorithm can halt is if 20 tests on the physical robot occur without triggering the stopping criterion described in equation 8: this event only occurred in 2 of 240 experiments performed on the physical robot described in the main text. In this case, we selected the highest-performing solution encountered

Table S1 Parameters of the reference controller.

Leg number		1	2	3	4	5	6
First joint	α_{i_1}	1.00	1.00	1.00	1.00	1.00	1.00
	ϕ_{i_1}	0.00	0.00	0.50	0.50	0.00	0.00
	τ_{i_1}	0.5	0.5	0.5	0.5	0.5	0.5
Two last joints	α_{i_2}	0.25	0.25	0.25	0.25	0.25	0.25
	ϕ_{i_2}	0.75	0.25	0.25	0.75	0.75	0.25
	τ_{i_2}	0.5	0.5	0.5	0.5	0.5	0.5

during the search. This user-defined stopping criterion is not strictly necessary, as the algorithm is guaranteed to stop in the worst case after every behavior in the map is tested, but it allows a practical limit on the number of trials performed on the physical robot.

Initiating the Adaptation Step The adaptation step is triggered when the performance drops by a certain amount. The simplest way to choose that threshold is to let the user specify it. Automating the selection of this value, and the impact of triggering the algorithm prematurely, is an interesting question for future research in this area.

Main parameters of MAP-Elites

- parameters in controller: 36
- parameter values (controller): 0 to 1, with 0.05 increments
- size of behavioral space: 6
- possible behavioral descriptors: $\{0, 0.25, 0.5, 0.75, 1\}$
- iterations: 40 million

Main parameters of M-BOA

- σ^2_{noise}: 0.001
- α: 0.9
- ρ: 0.4
- κ: 0.05

1.5 Robotic Arm Experiment

Physical robot The physical robot is a planar robotic arm with 8 degrees of freedom (Extended Data Fig. 7a) and a 1-degree-of-freedom gripper. The robot has to release a ball into a bin (a variant of the classic "pick and place" task in industrial robotics). To assess the position of the gripper, a red cap, placed on top of the gripper, is tracked with a video camera. The visual tracking is achieved with the "cmvision" ROS package, which tracks colored blobs (`http://wiki.ros.org/cmvision`). The eight joints of the robot are actuated by position-controlled servos manufactured by Dynamixel. To maximize the reliability of the the arm, the type of servo is not the same for all the joints: heavy-duty servos are used near the base of the robot and lighter ones are used for the end of the arm. The first joint, fixed to the base, is moved by two MX-28 servos mounted in parallel. The second joint is moved by an MX-64 servo. The 3 subsequent servos are single MX-28s, and the 3 remaining servos are AX-18s. All the robot's joints are limited to a motion range of $\pm\pi/2$.

Simulator The generation of the behavior-performance map is made with a simulated robot in the same way as for the hexapod experiment. For consistency with the simulated hexapod experiments, we used the dynamic (as opposed to kinematic) version of the simulator, based on the ODE library. Any joint configuration that resulted in the arm colliding with itself was not added to the map.

Parametrized controller The controller defines the target position for each joint. The controller is thus parametrized by eight continuous values from 0 to 1 describing the angle of each joint, which is mapped to the the total motion range of each joint of $\pm\pi/2$. The 8 joints are activated simultaneously and are driven to their target position by internal PID controllers.

We chose this simple control strategy to make the experiments easy to reproduce and highlight the contribution of Intelligent Trial & Error for damage recovery. More advanced control strategies, for instance visual servoing[27], would be more realistic in a industrial environment, but they would have made it hard to analyze the experimental results because both Intelligent Trial & Error and the controller would compensate for damage at the same time.

Randomly varying the controller's parameters Each parameter of the controller (section "Parametrized controller") has a 12.5% chance of being changed to any value from 0 to 1, with the new value chosen from a polynomial distribution as described on p. 124 of (Deb, 2000), with $\eta_m = 10.0$.

Behavioral descriptor Because the most important aspect of the robot's behavior in this task is the final position of the gripper, we use it as the behavioral descriptor:

$$\text{behavioral\_descriptor}(\text{simu}(\mathbf{c})) = \begin{bmatrix} x_g \\ y_g \end{bmatrix} \tag{9}$$

where (x_g, y_g) denotes the position of the gripper once all the joint have reached their target position.

The size of the working area of the robot is a rectangle measuring $1.4m \times 0.7m$. For the behavior-performance map, this rectangle is discretized into a grid composed of 20000 square cells (200×100). The robot is 62cm long.

Performance function Contrary to the hexapod experiment, for the robotic arm experiment the performance function for the behavior-map creation step and for the adaptation step are different. We did so to demonstrate that the two can be different, and to create a behavior-performance map that would work with arbitrary locations of the target bin.

For the *behavior-performance map generation step* (accomplished via the MAP-Elites algorithm), the performance function captures the

idea that all joints should contribute equally to the movement. Specifically, high-performance is defined as minimizing the variance of the joint angles, that is:

$$\text{performance}(\text{simu}(\mathbf{c})) = -\frac{1}{8}\sum_{i=0}^{i=7}\left(p_i - m\right)^2 \quad (10)$$

where p_i is the angular position of joint i (in radians) and $m = \frac{1}{8}\sum_{i=0}^{i=7} p_i$ is the mean of the joint angles. This performance function does not depend on the target. The map is therefore generic: it contains a high-performing controller for each point of the robot's working space.

For the *adaptation step* (accomplished via the M-BOA algorithm), the behavior-performance map, which is generic to many tasks, is used for a particular task. To do so, the adaption step has a different performance measure than the step that creates the behavior-performance map. For this problem, the predicted performance measure is the Euclidean distance to the target (closer is better). Specifically, for each behavior descriptor $\mathbf{x}$ in the map, performance is

$$\mathscr{P}(\mathbf{x}) = -||\mathbf{x} - \mathbf{b}|| \quad (11)$$

where $\mathbf{b}$ is the (x, y) position of the target bin. Note that the variance of the joint angles, which is used to create the behavior-performance map, is ignored during the adaptation step.

The performance of a controller on the physical robot is minimizing the Euclidean distance between the gripper (as measured with the external camera) and the target bin:

$$\text{performance}(\text{physical\_robot}(\mathscr{C}(\chi))) = -||\mathbf{x_g} - \mathbf{b}|| \quad (12)$$

where $\mathbf{x_g}$ is the position of the physical gripper after all joints have reached their final position, $\mathbf{b}$ is the position of the bin, and $\mathscr{C}(\chi)$ is the controller being evaluated (χ is the position in simulation that controller reached).

If the gripper reaches a position outside of the working area, then the camera cannot see the marker. In these rare cases, we set the performance of the corresponding controller to a low value (−1 m).

For the control experiments with traditional Bayesian optimization on the physical robot (see Supplementary Experiment S1), self-collisions are frequent during adaptation, especially given that we initialize the process with purely random controllers (i.e. random joint angles). While a single self-collision is unlikely to break the robot, hundreds of them can wear out the gearboxes because each servo continues to apply a force for a period of time until it determines that it cannot move. To minimize costs, and because we ran 210 independent runs of the algorithm (14 scenarios × 15 replicates), we first tested each behavior in simulation (taking the damage into account) to check that there were no self-collisions. If we detected a self-collision, the performance for that behavior was set to a low value (−1m).

Auto-collisions are much less likely with Intelligent Trial & Error because the behavior-performance map contains only controllers that do not self-collide on the undamaged, simulated robot. As a consequence, in the Intelligent Trial & Error experiments we did not simulate controllers before testing them on the physical robot.

Stopping criterion Because the robot's task is to release a ball into a bin, the adaptation step can be stopped when the gripper is above the bin. The bin is circular with a diameter of 10 cm, so we stopped the adaptation step when the red cap is within 5 cm of the center of the bin.

Main MAP-Elites parameters for the robotic arm experiment:

- parameters in controller: 8
- controller parameter values: 0 to 1 (continuous)
- dimensions in the behavioral space: 2
- simulated evaluations to create the behavior-performance map: 20 million

Main M-BOA parameters for the robotic arm experiment:

- σ^2_{noise}: 0.03
- ρ: 0.1
- κ: 0.3

1.6 Selection of parameters

All of the data reported in this section comes from experiments with the simulated hexapod robot, unless otherwise stated.

Selecting the ρ value For ρ between 0.1 and 0.8, we counted the number of behaviors from the map that would be influenced by a single test on the real hexapod robot (we considered a behavior to be influenced when its predicted performance was affected by more than 25% of the magnitude of the update for the tested behavior): with $\rho = 0.2$, the update process does not affect any neighbor in the map, with $\rho = 0.4$, it affects 10% of the behaviors, and with $\rho = 0.8$, it affects 80% of them. Additional values are shown in Supplementary Fig. 2c.

The previous paragraph describes tests we conducted to determine the number of behaviors in the map affected by different ρ values, but those experiments do not tell us how different ρ values affect the performance of the algorithm overall. To assess that, we then repeated the experiments from the main paper with a set of possible values ($\rho \in [0.1 : 0.025 : 0.8]$) in simulation (i.e., with a simulated, damaged robot), including testing on 6 separate damage scenarios (each where the robot loses a different leg) with all 8 independently generated replicates of the default 6-dimensional behavior-performance map. The algorithm stopped if 20 adaptation iterations passed without success according to the stopping criteria described in the main text and section 1.4: Stopping criterion. The results reveal that median performance decreases only modestly, but significantly, when the value of ρ increases: changing ρ from 0.1 to 0.8 only decreases the median value 12%, from 0.25 m/s to 0.22 m/s (p-value = 9.3×10^{-5} via Matlab's Wilcoxon ranksum test, Supplementary Fig. 2b). The variance in performance, especially at the extreme low end of the distribution of performance values, is not constant over the range of explored values. Around $\rho = 0.3$ the minimum performance (Supplementary Fig. 2b, dotted red line) is higher than the minimum performance for more extreme values of ρ.

A larger effect of changing ρ is the amount of time required to find a compensatory behavior, which decreases when the value of ρ increases (Supplementary Fig. 2b). With a ρ value lower than 0.25, the algorithm rarely converges in less than the allotted 20 iterations, which occurs because many more tests are required to cover all the promising areas of the search space to know if a higher-performing behavior exists than the best-already-tested. On the other hand, with a high ρ value, the algorithm updates its predictions for the entire search space in a few observations: while fast, this strategy risks missing promising areas of the search space.

In light of these data, we chose $\rho = 0.4$ as the default value for our hexapod experiments because it represents a good trade-off between a high minimum performance and a low number of physical tests on

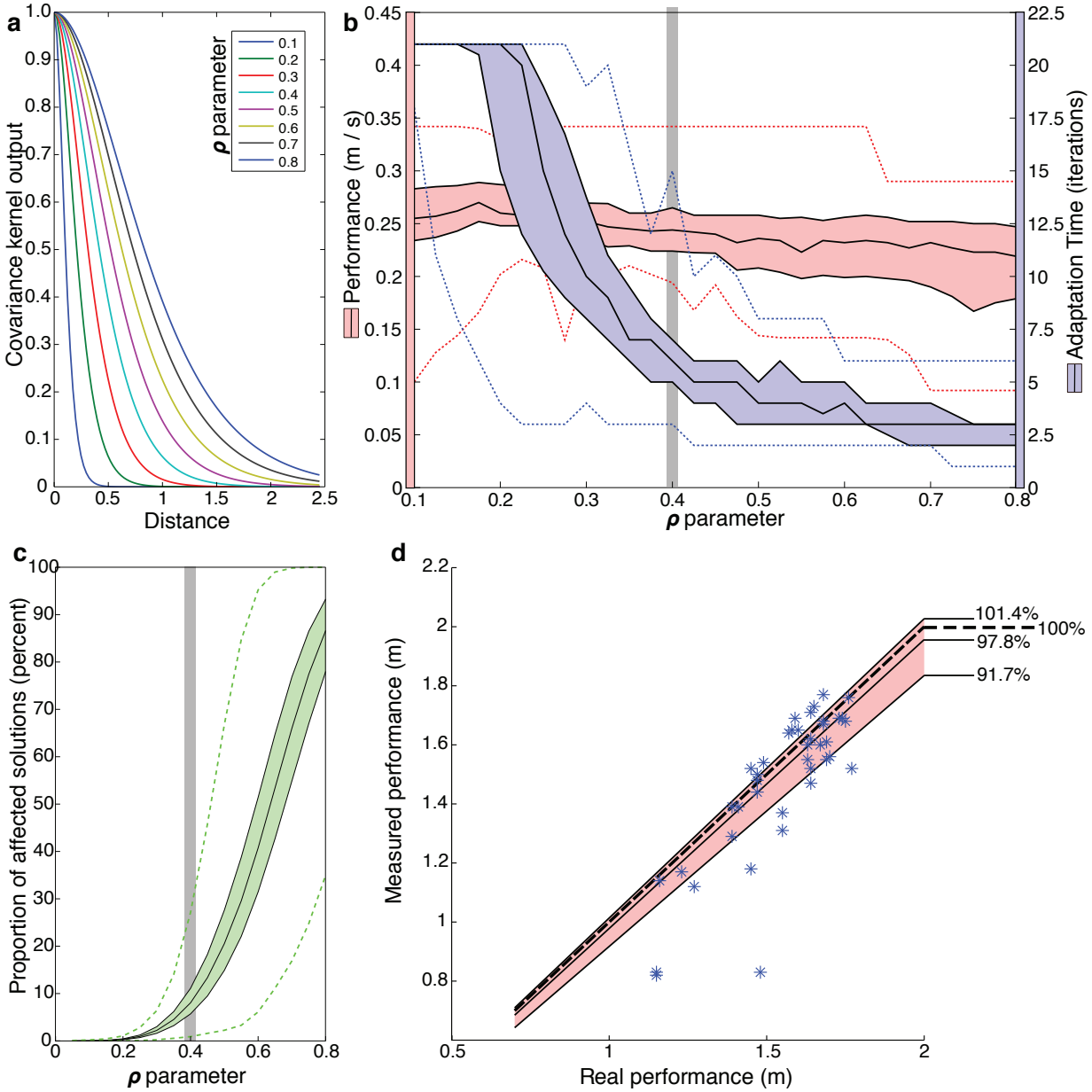

Supplementary Figure 2 | The effect of changing the algorithm's parameters. (a) The shape of the Matérn kernel function for different values of the ρ parameter. (b) Performance and required adaptation time obtained for different values of ρ. For each ρ value, the M-BOA algorithm was executed in simulation with 8 independently generated behavior-performance maps and for 6 different damage conditions (each case where one leg is missing). **(c) The number of controllers in the map affected by a new observation according to different values of the ρ parameter. (d) The precision of the odometry value**. The distances traveled by the physical robot, as measured manually ("real performance") is compared to the measurements automatically provided by the simultaneous location and mapping (SLAM) algorithm("measured performance"). The dashed black line indicates the hypothetical case where SLAM measurements are error-free and thus are the same as manual measurements. In (b), (c) and (d), the middle, black lines represent medians and the borders of the shaded areas show the 25th and 75th percentiles. The dotted lines are the minimum and maximum values. The gray bars show the ρ value chosen for the hexapod experiments in the main text.

the robot. The value of ρ for the robotic arm experiment has been chosen with the same method.

Selection of the κ value For the hexapod robot experiments, we chose $\kappa = 0.05$. This relatively low value emphasizes exploitation over exploration. We chose this value because the exploration of the search space has already been largely performed during the behavior-performance map creation step: the map suggests which areas of the space will be high-performing, and should thus be tested, and which areas of the space are likely unprofitable, and thus should be avoided.

For the robotic arm experiments, we chose $\kappa = 0.3$, which emphasizes exploration more, because it experimentally leads to better results.

1.7 Running time

Computing hardware All computation (on the physical robots and in simulation) was conducted on a hyperthreaded 16-core computer (Intel Xeon E5-2650 2.00GHz with 64Gb of RAM). This computational power is mainly required for the behavior-performance map creation step. Creating one map for the hexapod experiment took 2 weeks, taking advantage of the fact that map creation can easily be parallelized across multiple cores. Map creation only needs to be performed once per robot (or robot design), and can happen before the robot is deployed. As such, the robot's onboard computer does not need to be powerful enough to create the map.

For the hexapod robot experiment, the most expensive part of adaptation is the Simultaneous Localization And Mapping (SLAM) algorithm[20, 34, 35], which measures the distance traveled on the physical hexapod robot. It is slow because it processes millions of 3D points per second. It can be run on less powerful computers, but doing so lowers its accuracy because fewer frames per second can be processed. As computers become faster, it should be possible to run high-accuracy SLAM algorithms in low-cost, onboard computers for robots.

The rest of the adaptation step needs much less computational power and can easily be run on an onboard computer, such as a smartphone. That is because it takes approximately 15,000 arithmetic operations between two evaluations on the physical robot, which requires less than a second or two on current smartphones.

Measuring how long adaptation takes (hexapod robot) The reported time to adapt includes the time required for the computer to select each test and the time to conduct each test on the physical robot. Overall, evaluating a controller on the physical hexapod robot takes about 8 seconds (median 8.03 seconds, 5^{th} and 95^{th} percentiles [7.95; 8.21] seconds): 0.5-1 second to initialize the robot, 5 seconds during which the robot can walk, 0.5-1 second to allow the robot to stabilize before taking the final measurement, and 1-2 seconds to run the SLAM algorithm. Identifying the first controller to test takes 0.03 [0.0216; 0.1277] seconds. The time to select the next controller to test increases depending on the number of previous experiments because the size of the Kernel Matrix (K matrix, see Methods and Supplementary Fig. 1), which is involved in many of the arithmetic operations, grows by one row and one column per test that has been conducted. For example, selecting the second test takes 0.15 [0.13; 0.22] seconds, while the 10^{th} selection takes 0.31 [0.17; 0.34] seconds.

2 Supplementary Experiments S1

Additional conditions for the robotic arm

Methods We investigated 11 damage conditions on the physical robot in addition to the 3 described in the main text (Fig. 3). We used the same setup as described in the main text (see main text and section 1.5). Extended Data Fig. 7 shows the 14 scenarios.

For each of the 14 damage scenarios, we replicated experiments on the physical robot with 15 independently generated behavior-performance maps (210 runs in total). We also replicated control experiments, which consist of traditional Bayesian optimization directly in the original parameter space (i.e. without behavior-performance maps), 15 times for each of the 14 damage conditions (210 runs in total). For both the experimental and control treatments, each experiment involved 30 evaluations on the physical robot (31 if the first trial is counted). In many cases, not all 30 evaluations were required to reach the target, so we report only the number of trials required to reach that goal.

Results After running the MAP-Elites algorithm for 20 million evaluations, each of the 15 generated maps contain more than 11,000 behaviors (11,209 [1,1206; 1,1217] behaviors, Extended Data Fig. 7c).

In all the generated maps, the regions of different performance values for behaviors are arranged in concentric shapes resembling cardioids (inverted, heart-shaped curves) that cover the places the robot can reach (Extended Data Fig. 7c). The black line drawn over the shown map corresponds to all the positions of the end-effector for which all the degrees of freedom are set to the same angle (from $-\pi/4$ to $+\pi/4$), that is, for the theoretically highest achievable performance (i.e. the lowest possible variance in servo angles). The performance of the behaviors tends to decrease the further they are from this optimal line.

The adaptation results (Extended Data Fig. 7e) show that the Intelligent trial and error algorithm manages to reach the goal of being less than 5 cm from the center of the bin for all the runs in all the tested scenarios save two (scenarios 11 & 12). For these two scenarios, the algorithm still reaches the target 60% and 80% of the time, respectively. For all the damage conditions, the Intelligent Trial and Error algorithm reaches the target significantly more often than the Bayesian optimization algorithm ($p < 10^{-24}$). Specifically, the median number of iterations to reach the target (Extended Data Fig. 7f) is below 11 iterations (27.5 seconds) for all scenarios except 11 and 12, for which 31 and 20 iterations are required, respectively. When the robot is not able to reach the target, the recorded number of iterations is set to 31, which explains why the median number of iterations for the Bayesian optimization algorithm is equal to 31 for most damage conditions. For all the damage conditions except one (scenario 11), the Intelligent Trial and Error algorithm used fewer trials to reach the target than the traditional Bayesian optimization algorithm.

If the robot is allowed to continue its experiment after reaching the 5 cm radius tolerance, for a total of 31 iterations (Extended Data Fig. 7g), it reaches an accuracy around 1 cm for all the damage conditions except the two difficult ones (scenarios 11 and 12). This level of accuracy is never achieved with the classic Bayesian optimization algorithm, whose lowest median accuracy is $2.6cm$.

Scenarios 11 and 12 appear to challenge the Intelligent Trial and Error algorithm. While in both cases the success rate is improved, though not substantially, in case 11 the median accuracy is actually lower. These results stem from the fact that the difference between

the successful pre-damage and post-damage behaviors is so large that the post-damage solutions for both scenarios lie outside of the map. This illustrates a limit of the proposed approach: if the map does not contain a behavior able to cope with the damage, the robot will not be able to adapt. This limit mainly comes from the behavioral descriptor choice: we chose it because of its simplicity, but it does not capture all of the important dimensions of variation of the robot. More sophisticated descriptors are likely to allow the algorithm to cope with such situations. On the other hand, this experiment shows that with a very simple behavioral descriptor, using only the final position of the end-effector, our approach is able to deal with a large variety of different target positions and is significantly faster than the traditional Bayesian optimization approach (Extended Data Fig. 7d, maximum p-value over each time step $< 10^{-16}$), which is the current state of the art technique for direct policy search in robotics[3, 36, 16, 37].

3 Supplementary Experiments S2

The contribution of each subcomponent of the Intelligent Trial and Error Algorithm

Methods The Intelligent Trial and Error Algorithm relies on three main concepts: (1) the creation of a behavior-performance map in simulation via the MAP-Elites algorithm, (2) searching this map with a Bayesian optimization algorithm to find behaviors that perform well on the physical robot, and (3) initializing this Bayesian optimization search with the performance predictions obtained via the MAP-Elites algorithm: note that the second step could be performed without the third step by searching through the MAP-Elites-generated behavior-performance map with Bayesian optimization, but having the initial priors uniformly set to the same value. We investigated the contribution of each of these subcomponents by testing five variants of our algorithm : in each of them, we deactivated one of these three subcomponents or replaced it with an alternative algorithm from the literature. We then tested these variants on the hexapod robot. The variants are as follows:

- Variant 1 (MAP-Elites in 6 dimensions + random search): evaluates the benefit of searching the map via Bayesian optimization by searching that map with random search instead. Each iteration, a behavior is randomly selected from the map and tested on the robot. The best one is kept.
- Variant 2 (MAP-Elites in 6 dimensions + Bayesian optimization, no use of priors): evaluates the contribution of initializing the Gaussian process with the performance predictions of the behavior-performance map. In this variant, the Gaussian process is initialized with a constant mean (the average performance of the map: 0.24 m/s) at each location in the behavior space and a constant variance (the average variance of the map's performance: 0.005 m^2/s^2). As is customary, the first few trials (here, 5) of the Bayesian optimization process are selected randomly instead of letting the algorithm choose those points, which is known to improve performance.[16]
- Variant 3 (MAP-Elites in 6 dimensions + policy gradient): evaluates the benefit of Bayesian optimization compared to a more classic, local search algorithm[37, 38]; there is no obvious way to use priors in policy gradient algorithms.
- Variant 4 (Bayesian optimization in the original parameter space of 36 dimensions): evaluates the contribution of using a map in a lower-dimensional behavioral space. This variant searches directly in the original 36-dimensional parameter space instead of reducing that space to the lower-dimensional (six-dimensional) behavior space. Thus, in this variant no map of behaviors is produced ahead of time: the algorithm searches directly in the original, high-dimensional space. This variant corresponds to one of the best algorithms known to learn locomotion patterns[3, 16]. In this variant, the Gaussian process is initialized with a constant mean set to zero and with a constant variance ($0.002 m^2/s^2$). As described above, the five first trials are selected from pure random search to prime the Bayesian optimization algorithm[16].
- Variant 5 (Policy gradient in the original parameter space of 36 dimensions): a stochastic gradient descent in the original parameter space[38]. This approach is a classic reinforcement learning algorithm for locomotion[37] and it is a baseline in many papers[3].

It was necessary to compare these variants in simulation because doing so on the physical robot would have required months of experiments and would have repeatedly worn out or broken the robot. We modified the simulator from the main experiments (section 1.4: Simulator) to emulate 6 different possible damage conditions, each of which involved removing a different leg. For variants in which MAP-Elites creates a map (variants 1, 2 and 3), we used the same maps from the main experiments (the eight independently generated maps, which were all generated with a simulation of the undamaged robot): In these cases, we launched ten replicates of each variant for each of the eight maps and each of the six damage conditions. There are therefore $10 \times 8 \times 6 = 480$ replicates for each of those variants. For the other variants (4 and 5), we replicated each experiment 80 times for each of the six damage conditions, which also led to $80 \times 6 = 480$ replicates per variant. In all these simulated experiments, to roughly simulate the distribution of noisy odometry measurements on the real robot, the simulated performance values were randomly perturbed with a multiplicative Gaussian noise centered on 0.95 with a standard deviation of 0.1.

We analyze the fastest walking speed achieved with each variant after two different numbers of trials: the first case is after 17 trials, which was the maximum number of iterations used by the Intelligent Trial and Error Algorithm, and the second case is after 150 trials, which is approximately the number of trials used in previous work[38, 3, 16].

Results After 17 trials on the robot, Intelligent Trial and Error significantly outperforms all the variants (Extended Data Fig. 2b, $p < 10^{-67}$, Intelligent Trial and Error performance: 0.26 [0.20; 0.33] m/s), demonstrating that the three main components of the algorithm are needed to quickly find high-performing behaviors. Among the investigated variants, the random search in the map performs the best (Variant 1: 0.21 [0.16; 0.27] m/s), followed by Bayesian optimization in the map (Variant 2: 0.20 [0.13; 0.25] m/s), and policy gradient in the map (Variant 3: 0.13 [0; 0.23] m/s). Variants that search directly in the parameter space did not find any working behavior (Variant 4, Bayesian optimization: 0.04m/s, [0.01; 0.09]; Variant 5, policy gradient: 0.02 [0; 0.06] m/s).

There are two reasons that random search performs better than one might expect. First, the map only contains high-performing solutions, which are the result of the intense search of the MAP-Elites algorithm (40 million evaluations in simulation). The map thus already contains high-performing gaits of nearly every possible type. Therefore, this variant is not testing random controllers, but is randomly selecting high-performing solutions. Second, Bayesian optimization and policy gradient are not designed for such a low number of trials: without the priors on performance predictions introduced in the Intelligent Trial and Error Algorithm, the Bayesian optimization process needs to learn the overall shape of the search space to model it with a Gaussian process. 17 trials is too low a number to effectively sample six dimensions

(for a uniform sampling with only two possible values in each dimension, $2^6 = 64$ trials are needed; for five possible values, $5^6 = 15,625$ samples are needed). As a consequence, with this low number of trials, the Gaussian process that models the performance function is not informed enough to effectively guide the search. For the policy gradient algorithm, a gradient is estimated by empirically measuring the partial derivative of the performance function in each dimension. To do so, following[38], the policy gradient algorithm performs 15 trials at each iteration. Consequently, when only 17 trials are allowed, it iterates only once. In addition, policy gradient is a local optimization algorithm that highly depends on the starting point (which is here chosen randomly), as illustrated by the high variability in the performance achieved with this variant (Extended Data Fig. 2b).

The issues faced by Bayesian optimization and policy gradient are exacerbated when the algorithms search directly in the original, 36-dimensional parameter space instead of the lower-dimensional (six-dimensional) behavior space of the map. As mentioned previously, no working controller was found in the two variants directly searching in this high-dimensional space.

Overall, the analysis after 17 trials shows that:

- The most critical component of the Intelligent Trial and Error Algorithm is the MAP-Elites algorithm, which reduces the search space and produces a map of high-performing behaviors in that space: $p < 5 \times 10^{-50}$ when comparing variants searching in the behavior-performance map space vs. variants that search in the original, higher-dimensional space of motor parameters.
- Bayesian optimization critically improves the search, but only when it is initialized with the performance obtained in simulation during the behavior-performance map creation step (with initialization: 0.26 [0.20; 0.33] m/s, without initialization: 0.20 [0.13; 0.25] m/s, $p = 10^{-96}$).

To check whether these variants might perform better if allowed the number of evaluations typically given to previous state-of-the-art algorithms[38, 3, 16], we continued the experiments until 150 trials on the robot were conducted (Extended Data Fig. 2c). Although the results for all the variants improved, Intelligent Trial and Error still outperforms all them ($p < 10^{-94}$; Intelligent Trial and Error: 0.31 [0.26; 0.37] m/s, random search: 0.26 [0.22; 0.30] m/s, Bayesian optimization: 0.25 [0.18; 0.31] m/s, policy search: 0.23 [0.19, 0.29] m/s). These results are consistent with the previously published results[38, 3, 16, 37], which optimize in 4 to 10 dimensions in a few hundred trials. Nevertheless, when MAP-Elites is not used, i.e. when we run these algorithms in the original 36 dimensions for 150 evaluations, Bayesian optimization and policy gradient both perform much worse (Bayesian optimization: 0.08 [0.05; 0.12]; policy gradient: 0.06 [0.01; 0.12] m/s). These results shows that MAP-Elites is a powerful method to reduce the dimensionality of a search space for learning algorithms, in addition to providing helpful priors about the search space that speed up Bayesian optimization.

Overall, these additional experiments demonstrate that each of the three main components of the Intelligent Trial and Error Algorithm substantially improves performance. The results also indicate that Intelligent Trial and Error significantly outperforms previous algorithms for both damage recovery [39, 40, 41, 42, 43] and gait learning [44, 38, 45, 22, 46, 3, 36, 16, 37, 23], and can therefore be considered the state of the art.

4 Supplementary Experiments S3

Robustness to environmental changes

Methods The map creation algorithm (MAP-Elites) uses an undamaged robot on flat terrain. The main experiments show that this algorithm provides useful priors for damage recovery on a flat terrain. In these supplementary experiments, we evaluated, in simulation, if the map created on flat terrain also provides a useful starting point for discovering gaits for sloped terrains.

We first evaluated the effect slopes have on undamaged robots (Extended Data Fig. 3a). We launched 10 replicates for each of the eight maps and each one-degree increment between $-20°$ and $+20°$, for a total of $10 \times 8 \times 41 = 3280$ experiments. As in Supplementary Experiments S2, to roughly simulate the distribution of noisy odometry measurements on the real robot, we perturbed performance values with a multiplicative Gaussian noise centered on 0.95 with a standard deviation of 0.1.

Results The results show that, when the slope is negative (descending), the Intelligent Trial and Error approach finds fast gaits in fewer than than 3 trials. For reference, a hand-designed, classic, tripod gait (section 1.4) falls on slopes below $-15°$ degrees. When the slope is positive (ascent), Intelligent Trial and Error finds slower behaviors, as is expected, but even above $10°$ the gait learned by Intelligent Trial and Error outperforms the reference gait on flat ground. Overall, for every slope angle, the controller found by Intelligent Trial and Error is faster than the hand-designed reference controller.

We further evaluated damage recovery performance for these same slopes with the same setup as Experiments S2 (6 damage conditions). We launched 10 replicates for each damage condition, for 8 independently generated behavior-performance maps, and each two-degree increment between $-20°$ and $+20°$ degrees. There are therefore 480 replicates for each two-degree increment between $-20°$ and $+20°$, for a total of $480 \times 21 = 10080$ experiments.

Intelligent Trial and Error is not critically affected by variations of slope between $-10°$ and $+10°$ (Extended Data Fig. 3b): for these slopes, and for all 6 damage conditions, Intelligent Trial and Error finds fast gaits (above 0.2 m/s) in less than 15 tests on the robot despite the slope. As expected, it finds faster gaits for negative slopes (descent) and slower gaits for positive slopes (ascent). For slopes below $-10°$ and above $10°$, the algorithm performs worse and requires more trials. These results likely are caused by the constraints placed on the controller and the limited sensors on the robot, rather than the inabilities of the algorithm. Specifically, the controller was kept simple to make the science clearer, more intuitive, and more reproducible. Those constraints, of course, prevent it from performing the more complex behaviors necessary to deal with highly sloped terrain. For example, the constraints prevent the robot from keeping its legs vertical on sloped ground, which would substantially reduce slippage. Nevertheless, the median Intelligent Trial and Error compensatory gait still outperforms the median performance of the reference gait on all slope angles.

5 Supplementary Experiments S4

Comparison between MAP-Elites and Random Sampling

Methods The MAP-Elites algorithm is a stochastic search algorithm that attempts to fill a discretized map with the highest-performing solution at each point in the map. As explained in the main text, each point in the map represents a different type of behavior, as defined by the behavioral dimension of the map. MAP-Elites generates new candidate points by randomly selecting a location in the map, changing the parameters of the controller that is stored there, and then saving that controller in the appropriate map location if it is better than the current occupant at that location. Intuitively, generating new candidate solutions from the best solutions found so far should be better than generating a multitude of controllers randomly and then keeping the best one found for each location in the map. In this section we report on experiments that confirm that intuition.

To understand the advantages of MAP-Elites over random sampling, we compared the two algorithms by generating data with the simulated hexapod. The experiments have the same virtual robot, environment, controller, performance function, and behavioral descriptors as in the main experiments (see Methods). We analyzed the number of cells for which a solution is found (an indication of the diversity of behavior types the algorithms generate), the average performance of behaviors in the map, and the maximum performance discovered.

We replicated each experiment 8 times, each of which included 20 million evaluations on the simulated robot.

Results The results show that the MAP-Elites algorithm outperforms random sampling on each of these measures (Supplementary Fig. 3). After 20 million evaluations, about 13000 cells (median: 12968, 5^{th} & 95^{th} percentiles: [12892; 13018]) are filled by MAP-Elites (about 83% percent of the map), whereas random sampling only filled approximately 8600 (8624 [8566; 8641]) cells (about 55% percent of the map) (Supplementary Fig. 3a). The difference between the two algorithms is large and appears early (Supplementary Fig. 3a); after only 1 million evaluations, MAP-Elites filled 10670 [10511; 10775] cells (68% of the map), whereas random sampling filled 5928 [5882; 5966] cells (38% of the map).

The solutions discovered by MAP-Elites are not only more numerous, but also outperform those found by random sampling (Supplementary Fig. 3b): with MAP-Elites, after 20 million evaluations the average performance of filled cells is 0.22 [0.22; 0.23] m/s, whereas it is 0.06 [0.06; 0.06] m/s with random sampling, which is similar to the performance obtained with the reference controller on a damaged robot (Fig. 3). These two results demonstrate that MAP-Elites is a much better algorithm than random sampling to find a map of the diverse, "elite" performers in a search space.

In addition, MAP-Elites is a better optimization algorithm, as measured by the performance of the best single solution produced. The performance of the best solution in the map after 20 million evaluations is 0.40 [0.39;0.41] m/s with MAP-Elites, compared to 0.21 [0.20; 0.22] m/s with random sampling.

6 Supplementary Experiments S5

Alternative behavioral descriptors

Methods To create a map with MAP-Elites, one has to define the dimensions of the behavioral space, i.e. the behavioral descriptors. The main experiments show that using a predefined behavioral descriptor (the proportion of time that each leg of a hexapod robot is in contact with the ground, i.e. the duty factor) creates a map that provides useful priors for damage recovery.

This section describes how we tested (in simulation) how performance is affected by alternative behavioral descriptors, including descriptors that have a different number of dimensions. We also evaluated how performance is affected if the behavioral descriptors are randomly selected from a large list of potential descriptors. This test simulates the algorithm's performance if the behavioral descriptors are chosen without insight into the problem domain.

The behavioral descriptors we tested are as follows:

1. Duty factor (6-dimensional): This descriptor is the default one from the main experiment. It corresponds to the proportion of time each leg is in contact with the ground:

$$\mathbf{x} = \begin{bmatrix} \frac{\sum_t C_1(t)}{\text{numTimesteps}} \\ \vdots \\ \frac{\sum_t C_6(t)}{\text{numTimesteps}} \end{bmatrix} \tag{13}$$

   where $C_i(t)$ denotes the Boolean value of whether leg i is in contact with the ground at time t (1: contact, 0: no contact).

2. Orientation (6-dimensional): This behavioral descriptor characterizes changes in the angular position of the robot during walking, measured as the proportion of 15ms intervals that each of the pitch, roll and yaw angles of the robot frame are positive (three dimensions) and negative (three additional dimensions):

$$\mathbf{x} = \begin{bmatrix} \frac{1}{K}\sum_k U(\Theta^T(k) - 0.005\pi) \\ \frac{1}{K}\sum_k U(-\Theta^T(k) - 0.005\pi) \\ \frac{1}{K}\sum_k U(\Psi^T(k) - 0.005\pi) \\ \frac{1}{K}\sum_k U(-\Psi^T(k) - 0.005\pi) \\ \frac{1}{K}\sum_k U(\Phi^T(k) - 0.005\pi) \\ \frac{1}{K}\sum_k U(-\Phi^T(k) - 0.005\pi) \end{bmatrix} \tag{14}$$

   where $\Theta^T(k)$, $\Psi^T(k)$ and $\Phi^T(k)$ denote the pitch, roll and yaw angles, respectively, of the robot torso (hence T) at the end of interval k, and K denotes the number of 15ms intervals during the 5 seconds of simulated movement (here, $K = 5s/0.015s \approx 334$). The unit step function $U(\cdot)$ returns 1 if its argument exceeds 0, and returns 0 otherwise. To discount for insignificant motion around 0 rad, orientation angles are only defined as positive if they exceed 0.5% of π rad. Similarly, orientation angles are only defined as negative if they are less than -0.5% of π rad.

3. Displacement (6-dimensional): This behavioral descriptor characterizes changes in the postion of the robot during walking. It is measured as the proportion of 15ms intervals that the robot is positively or negatively displaced along each of the x, y, and z axes:

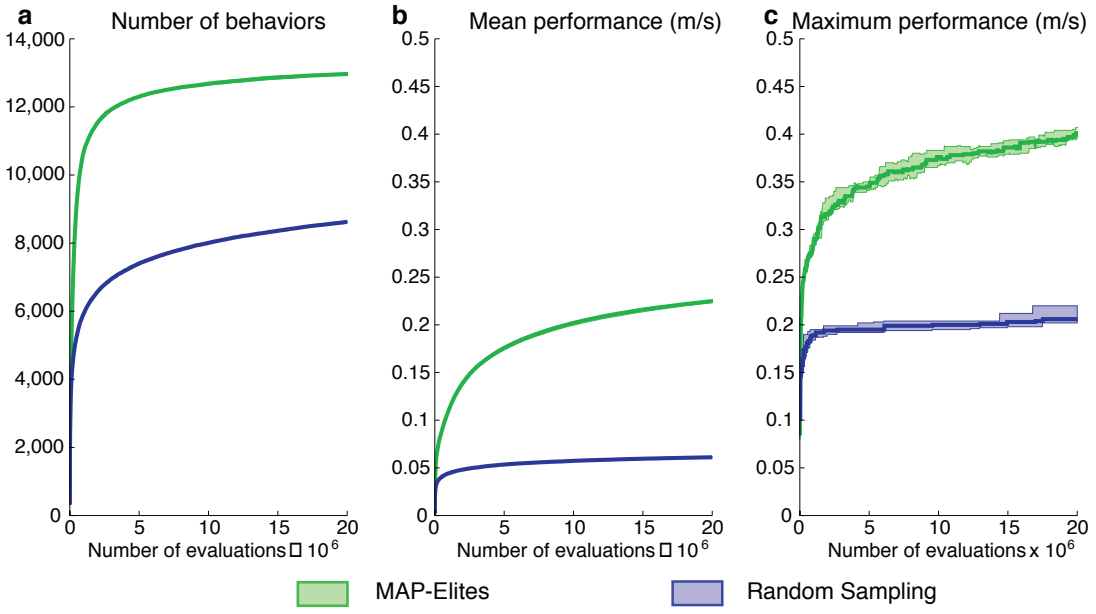

Supplementary Figure 3 | Comparing MAP-Elites and random sampling for generating behavior-performance maps. (a) The number of points in the map for which a behavior is discovered. (b) The mean performance of the behaviors in the map. (c) The maximum performance of the behaviors in the map. For all these figures, the middle lines represent medians over 8 independently generated maps and the shaded regions extend to the 25$^{\text{th}}$ and 75$^{\text{th}}$ percentiles, even for (a) and (b), where the variance of the distribution is so small that it is difficult to see. See Supplementary Experiment S4 for methods and analysis.

$$\mathbf{x} = \begin{bmatrix} \frac{1}{K}\sum_k U(\Delta x(k) - 0.001) \\ \frac{1}{K}\sum_k U(-\Delta x(k) - 0.001) \\ \frac{1}{K}\sum_k U(\Delta y(k) - 0.001) \\ \frac{1}{K}\sum_k U(-\Delta y(k) - 0.001) \\ \frac{1}{K}\sum_k U(\Delta z(k) - 0.001) \\ \frac{1}{K}\sum_k U(-\Delta z(k) - 0.001) \end{bmatrix} \quad (15)$$

where $[\Delta x(k), \Delta y(k), \Delta z(k)]$ denote the linear displacement in meters of the robot during interval k, and K denotes the number of 15ms intervals during 5 seconds of simulated movement (here, $K = 5s/0.015s \approx 334$). The unit step function $U(\cdot)$ returns a value of 1 if its argument exceeds 0, and returns a value of 0 otherwise. To ignore insignificant motion, linear displacements are defined to be positive if they exceed 1mm, and are defined to be negative if they are less than −1mm.

4. Total energy expended per leg (6-dimensional): This behavioral descriptor captures the total amount of energy expended to move each leg during 5 seconds of movement:

$$\mathbf{x} = \begin{bmatrix} \frac{E_1}{M_E} \\ \vdots \\ \frac{E_6}{M_E} \end{bmatrix} \quad (16)$$

where E_i denotes the energy utilized by leg i of the robot during 5 seconds of simulated movement, measured in N.m.rad. M_E is the maximum amount of energy available according to the servo model of the simulator, which for 5 seconds is 100 N.m.rad.

5. Relative energy expended per leg (6-dimensional): This behavioral descriptor captures the amount of energy expended to move each leg relative to the energy expended by all the legs during 5 seconds of simulated movement:

$$\mathbf{x} = \begin{bmatrix} \frac{E_1}{\sum_{i=1..6} E_i} \\ \vdots \\ \frac{E_6}{\sum_{i=1..6} E_i} \end{bmatrix} \quad (17)$$

where E_i denotes the energy utilized by leg i of the robot during 5 seconds of simulated movement, measured in N.m.rad.

6. Deviation (3-dimensional): This descriptor captures the range of deviation of the center of the robot frame versus the expected location of the robot if it traveled in a straight line at a constant speed.

$$\mathbf{x} = \begin{bmatrix} \frac{0.95\left(\max_t(x(t)) - \min_t(x(t))\right)}{0.2} \\ \frac{0.95\left(\max_t(y(t) - \frac{y_{\text{final}}}{5} \times t) - \min_t(y(t) - \frac{y_{\text{final}}}{5} \times t)\right)}{0.2} \\ \frac{0.95\left(\max_t(z(t)) - \min_t(z(t))\right)}{0.2} \end{bmatrix} \quad (18)$$

where $[x(t), y(t), z(t)]$ denote the position of robot's center at time t, and $[x_{\text{final}}, y_{\text{final}}, z_{\text{final}}]$ denote its final position after 5 seconds.

The robot's task is to move along the y-axis. Its starting position is (0,0,0). The deviation along the x and z axes is computed as the maximum difference in the robot's position in those dimensions at any point during 5 seconds. For the y axis, $\frac{y_{\text{final}}}{5}$ corresponds to the average speed of the robot (the distance covered divided by total time), therefore $\frac{y_{\text{final}}}{5} \times t$ is the expected position at timestep t if the robot was moving at constant speed. The deviation from

the y axis is computed with respect to this "theoretical" position.

To obtain values in the range [0,1], the final behavioral descriptors are multiplied by 0.95 and then divided by 20 cm (these values were determined empirically).

7. Total ground reaction force per leg (6-dimensional): This behavioral descriptor corresponds to the amount of force each leg applies to the ground, measured as a fraction the total possible amount of force that a leg could apply to the ground. Specifically, the measurement is

$$\mathbf{x} = \begin{bmatrix} \frac{F_1}{M_F} \\ \vdots \\ \frac{F_6}{M_F} \end{bmatrix} \tag{19}$$

where F_i denotes the ground reaction force (GRF) each leg i generates, averaged over 5 seconds of simulated movement. M_F is the maximum such force that each leg can apply, which is 10N.

8. Relative ground reaction force per leg (6-dimensional): This behavioral descriptor corresponds to the amount of force each leg applies to the ground, relative to that of all the legs:

$$\mathbf{x} = \begin{bmatrix} \frac{F_1}{\sum_{i=1..6} F_i} \\ \vdots \\ \frac{F_6}{\sum_{i=1..6} F_i} \end{bmatrix} \tag{20}$$

where F_i denotes the ground reaction force (GRF) each leg i generates, averaged over 5 seconds of simulated movement.

9. Lower-leg pitch angle (6-dimensional): This descriptor captures the pitch angle for the lower-leg with respect to the ground (in a global coordinate frame), averaged over 5 seconds:

$$\mathbf{x} = \begin{bmatrix} \frac{\sum_t \Theta_1^L(t)}{\pi \times N_1} \\ \vdots \\ \frac{\sum_t \Theta_6^L(t)}{\pi \times N_6} \end{bmatrix} \tag{21}$$

where $\Theta_i^L(t)$ is the pitch angle of lower-leg i (hence the L in Θ_i^L) when it is in contact with the ground at time t, and N_i is the number of time-steps for which lower-leg i touches the ground. The foot pitch angles are in range $[0,\pi]$ (as the leg can not penetrate the ground) and normalized to $[0,1]$.

10. Lower-leg roll angle (6-dimensional): This descriptor captures the roll angle for the lower-leg with respect to the ground (in a global coordinate frame), averaged over 5 seconds:

$$\mathbf{x} = \begin{bmatrix} \frac{\sum_t \Psi_1^L(t)}{\pi \times N_1} \\ \vdots \\ \frac{\sum_t \Psi_6^L(t)}{\pi \times N_6} \end{bmatrix} \tag{22}$$

where $\Psi_i^L(t)$ is the roll angle of lower-leg i (hence L in Ψ_i^L) when it is in contact with the ground at time t, and N_i is the number of time-steps for which lower-leg i touches the ground. The foot roll angles are in range $[0,\pi]$ (as the leg can not penetrate the ground) and normalized to $[0,1]$.

11. Lower-leg yaw angle (6-dimensional): This descriptor captures the yaw angle for the lower-leg with respect to the ground (in a global coordinate frame), averaged over 5 seconds:

$$\mathbf{x} = \begin{bmatrix} \frac{\sum_t \Phi_1^L(t)+\pi}{2\pi \times N_1} \\ \vdots \\ \frac{\sum_t \Phi_6^L(t)+\pi}{2\pi \times N_6} \end{bmatrix} \tag{23}$$

where $\Phi_i^L(t)$ is the yaw angle of lower-leg i (hence L in Φ_i^L) when it is in contact with the ground at time t,and N_i is the number of time-steps for which lower-leg i touches the ground. The foot yaw angles are in range $[-\pi,\pi]$ and are normalized to $[0,1]$.

12. Random (6-dimensional): The random behavioral descriptor differs from the other intentionally chosen descriptors in that it does not consist of one type of knowledge, but is instead randomly selected as a subset of variables from the previously described 11 behavioral descriptors. This descriptor is intended to simulate a situation in which one has little expectation for which behavioral descriptor will perform well, so one quickly picks a few different descriptor dimensions without consideration or experimentation. Instead of generating one such list in this fashion, we randomly sample from a large set to find the average performance of this approach over many different possible choices.

    For the random descriptor, each of the 6-dimensions is selected at random (without replacement) from the $1\times3+10\times6=63$ available behavior descriptor dimensions described in the previous 11 descriptors (1 of the above descriptors is three-dimensional and the other 10 are six-dimensional):

$$\mathbf{x} = \begin{bmatrix} R_1 \\ \vdots \\ R_6 \end{bmatrix} \tag{24}$$

    where R_i denotes the i^{th} dimension of the descriptor, randomly selected uniformly and without replacement from the 63 available dimensions in behavior descriptors 1-11.

It was necessary to compare these behavioral descriptors in simulation because doing so on the physical robot would have required months of experiments and would have repeatedly worn out or broken the robot. We modified the simulator from the main experiments (section 1.4) to emulate 6 different possible damage conditions, each of which involved removing a different leg. The MAP-Elites algorithm, run for 3 million iterations, was used to create the behavior-performance maps for each of the behavioral descriptors (using a simulation of the undamaged robot). During the generation of the behavior-performance maps, the behaviors were stored in the map's cells by discretizing each dimension of the behavioral descriptor space with these five values: $\{0, 0.25, 0.5, 0.75, 1\}$ for the 6-dimensional behavioral descriptors, and with twenty equidistant values between $[0,1]$ for the 3-dimensional behavioral descriptor. During the adaptation phase, the behaviors were used with their actual values and thus not discretized.

We independently generated eight maps for each of the 11 intentionally chosen behavioral descriptors. Twenty independently generated maps were generated for the random behavioral descriptor. We launched ten replicates of each descriptor for each of the maps (eight for intentionally chosen behavioral descriptors and twenty for random behavioral descriptor) and each of the six damage conditions. There

are therefore $10 \times 8 \times 6 = 480$ replicates for each of the intentionally chosen descriptors, and $10 \times 20 \times 6 = 1200$ replicates for the random descriptor. In all these simulated experiments, to roughly simulate the distribution of noisy odometry measurements on the real robot, the simulated performance values were randomly perturbed with a multiplicative Gaussian noise centered on 0.95 with a standard deviation of 0.1.

We analyze the fastest walking speed achieved with each behavioral descriptor after two different numbers of trials: the first case is after 17 trials, and the second case is after 150 trials.

Results The following results include 17 trials on the simulated robot, which was the maximum number of trials required for Intelligent Trial and Error to find a compensatory gait in the Supplementary Experiment S2. The post-adaptation performance achieved with our alternative, intentionally chosen behavioral descriptors (numbers 2-11) was similar to the original duty factor behavioral descriptor (number 1) (Extended Data Fig. 4a). All 11 alternative, intentionally chosen descriptors (numbers 2-11) led to a median performance within 17% of the duty factor descriptor (performance: 0.241 [0.19; 0.29] m/s). The difference in performance was effectively nonexistent with the deviation descriptor (0.241 [0.14; 0.31] m/s), the total GRF descriptor (0.237 [0.15; 0.30] m/s), and the lower-leg roll angle descriptor (0.235 [0.14; 0.31] m/s). The lowest performance was discovered with the relative GRF descriptor (16.7% lower than the duty factor descriptor, 0.204 [0.08; 0.31] m/s). In terms of statistical significance, the performance achieved with the duty factor descriptor was no different from the deviation ($p = 0.53$) and total GRF ($p = 0.29$) descriptors. With all the remaining descriptors, the difference in performance was statistically significant ($p < 10^{-3}$), but it did not exceed 0.04m/s. Additionally, the compensatory behaviors discovered with all our 11 alternative, intentionally chosen descriptors were always faster than the reference gait for all damage conditions.

To check whether our alternative, intentionally chosen behavioral descriptors lead to better performance if allowed a higher number of evaluations, we extended the experiments to 150 trials on the robot (Extended Data Fig. 4b). After 150 trials, the difference in performance between the duty factor behavioral descriptor (0.277 [0.24; 0.34] m/s) and our alternative behavioral descriptors was further reduced. For all but three alternative, intentionally chosen descriptors (displacement, total GRF and lower-leg yaw angle), the median performance was within 4% of the duty factor descriptor. The difference in performance was at ±3.6% with the orientation (0.274 [0.22; 0.32] m/s), total energy (0.274 [0.19; 0.33] m/s), relative energy (0.273 [0.20; 0.32] m/s), deviation (0.287 [0.21; 0.34] m/s), relative GRF (0.266 [0.15; 0.35] m/s), lower-leg pitch angle (0.271 [0.21; 0.34] m/s) and lower-leg roll angle (0.268 [0.17; 0.34] m/s) descriptors. In the three remaining behavioral descriptors, displacement, total GRF, and lower-leg yaw angle, the performance was 0.264 [0.18; 0.32] m/s, 0.299 [0.25; 0.35] m/s and 0.255 [0.18; 0.32] m/s, respectively (difference at ±7.8% of duty factor descriptor in all three cases). In terms of statistical significance, the performance achieved with the duty factor descriptor was barely statistically significantly different from the deviation descriptor ($p = 0.041$). In all the remaining descriptors, the performance difference was statistically significant ($p < 10^{-2}$), but no larger than 0.02m/s.

Our random behavioral descriptor also performed similarly to the duty factor descriptor. After 17 trials, the performance of M-BOA with the maps generated by the random descriptor was 0.232 [0.14; 0.30] m/s (4.2% lower than the duty factor descriptor performance). While the difference is statistically significant ($p < 10^{-3}$), the difference in performance itself was negligible at 0.01m/s. This difference in performance was further reduced to 3.6% after 150 trials (random descriptor performance: 0.274 [0.21; 0.34] m/s, duty factor description performance: 0.277 [0.24; 0.34] m/s, $p = 0.002$). Moreover, as with the intentionally chosen behavioral descriptors, the compensatory behavior discovered with the random descriptor was also faster than the reference gait.

These experiments show that the selection of the behavioral dimensions is not critical to get good results. Indeed, all tested behavioral descriptors, even those randomly generated, perform well (median > 0.20 m/s after 17 trials). On the other hand, if the robot's designers have some prior knowledge about which dimensions of variation are likely to reveal different types of behaviors, the algorithm can benefit from this knowledge to further improve results (as with the duty factor descriptor).

7 Caption for Supplementary Videos

Video S1

Damage Recovery in Robots via Intelligent Trial and Error. The video shows the Intelligent Trial and Error Algorithm in action with the two robots introduced in this paper: the hexapod robot and the 8 degrees of freedom robotic arm (Fig. 3). The video shows several examples of the different types of behaviors that are produced during the behavior-performance map creation step, from classic hexapod gaits to more unexpected forms of locomotion. Then, it shows how the hexapod robot uses that behavior-performance map to deal with a leg that has lost power (Fig. 3a:C3). Finally, the video illustrates how the Intelligent Trial and Error Algorithm can be applied to the second robot and to different damage conditions.

Video S2

A Behavior-Performance Map Containing Many Different Types of Walking Gaits. In the behavior-performance map creation step, the MAP-Elites algorithm produces a collection of different types of walking gaits. The video shows several examples of the different types of behaviors that are produced, from classic hexapod gaits to more unexpected forms of locomotion.

Supplementary References

1. Eiben, A. E. & Smith, J. E. *Introduction to evolutionary computing* (Springer, 2003).
2. Mouret, J.-B. & Clune, J. Illuminating search spaces by mapping elites. *arXiv preprint arXiv:1504.04909* (2015).
3. Lizotte, D. J., Wang, T., Bowling, M. H. & Schuurmans, D. Automatic gait optimization with gaussian process regression. In *Proceedings of the the International Joint Conference on Artificial Intelligence (IJCAI)*, vol. 7, 944–949 (2007).
4. Brochu, E., Cora, V. M. & De Freitas, N. A tutorial on bayesian optimization of expensive cost functions, with application to active user modeling and hierarchical reinforcement learning. *arXiv preprint arXiv:1012.2599* (2010).
5. Mockus, J. *Bayesian approach to global optimization: theory and applications* (Kluwer Academic, 2013).
6. Snoek, J., Larochelle, H. & Adams, R. P. Practical bayesian optimization of machine learning algorithms. In *Advances in Neural Information Processing Systems 25 (NIPS)*, 2951–2959 (2012).

7. Griffiths, T. L., Lucas, C., Williams, J. & Kalish, M. L. Modeling human function learning with gaussian processes. In *Advances in Neural Information Processing Systems 21 (NIPS)*, 553–560 (2009).
8. Borji, A. & Itti, L. Bayesian optimization explains human active search. In *Advances in Neural Information Processing Systems 26 (NIPS)*, 55–63 (2013).
9. Booker, A. J. *et al.* A rigorous framework for optimization of expensive functions by surrogates. *Structural optimization* **17**, 1–13 (1999).
10. Forrester, A. I. J. & Keane, A. J. Recent advances in surrogate-based optimization. *Progress in Aerospace Sciences* **45**, 50–79 (2009).
11. Jin, Y. Surrogate-assisted evolutionary computation: Recent advances and future challenges. *Swarm and Evolutionary Computation* **1**, 61–70 (2011).
12. Simpson, T. W., Mauery, T. M., Korte, J. J. & Mistree, F. Comparison of response surface and kriging models for multidisciplinary design optimization. *American Institute of Aeronautics and Astronautics* **98**, 1–16 (1998).
13. Jones, D. R., Schonlau, M. & Welch, W. J. Efficient global optimization of expensive black-box functions. *Journal of Global optimization* **13**, 455–492 (1998).
14. Sacks, J., Welch, W. J., Mitchell, T. J., Wynn, H. P. *et al.* Design and analysis of computer experiments. *Statistical science* **4**, 409–423 (1989).
15. Rasmussen, C. E. & Williams, C. K. I. *Gaussian processes for machine learning* (MIT Press, 2006).
16. Calandra, R., Seyfarth, A., Peters, J. & Deisenroth, M. P. An experimental comparison of bayesian optimization for bipedal locomotion. In *Proceedings of the IEEE International Conference on Robotics and Automation (ICRA)* (2014).
17. Matérn, B. *et al.* Spatial variation. stochastic models and their application to some problems in forest surveys and other sampling investigations. *Meddelanden fran statens Skogsforskningsinstitut* **49** (1960).
18. Stein, M. L. *Interpolation of spatial data: some theory for kriging* (Springer, 1999).
19. Fiacco, A. V. & McCormick, G. P. *Nonlinear programming: sequential unconstrained minimization techniques*, vol. 4 (Siam, 1990).
20. Dryanovski, I., Valenti, R. G. & Xiao, J. Fast visual odometry and mapping from rgb-d data. In *Proceedings of the IEEE International Conference on Robotics and Automation (ICRA)*, 2305–2310 (IEEE, 2013).
21. Quigley, M. *et al.* ROS: an open-source robot operating system. In *Proceedings of ICRA's workshop on Open Source Software* (2009).
22. Sproewitz, A., Moeckel, R., Maye, J. & Ijspeert, A. Learning to move in modular robots using central pattern generators and online optimization. *The International Journal of Robotics Research* **27**, 423–443 (2008).
23. Yosinski, J. *et al.* Evolving Robot Gaits in Hardware: the HyperNEAT Generative Encoding Vs. Parameter Optimization. *Proceedings of ECAL* 890–897 (2011).
24. Clune, J., Stanley, K., Pennock, R. & Ofria, C. On the performance of indirect encoding across the continuum of regularity. *IEEE Transactions on Evolutionary Computation* **15**, 346–367 (2011).
25. Clune, J., Beckmann, B., Ofria, C. & Pennock, R. Evolving coordinated quadruped gaits with the HyperNEAT generative encoding. In *Proceedings of the IEEE Congress on Evolutionary Computation*, 2764–2771 (2009).
26. Lee, S., Yosinski, J., Glette, K., Lipson, H. & Clune, J. Evolving gaits for physical robots with the hyperneat generative encoding: the benefits of simulation. In *Applications of Evolutionary Computing* (Springer, 2013).
27. Siciliano, B. & Khatib, O. *Springer handbook of robotics* (Springer, 2008).
28. Wilson, D. Insect walking. *Annual Review of Entomology* **11**, 103–122 (1966).
29. Saranli, U., Buehler, M. & Koditschek, D. Rhex: A simple and highly mobile hexapod robot. *The International Journal of Robotics Research* **20**, 616–631 (2001).
30. Schmitz, J., Dean, J., Kindermann, T., Schumm, M. & Cruse, H. A biologically inspired controller for hexapod walking: simple solutions by exploiting physical properties. *The biological bulletin* **200**, 195–200 (2001).
31. Ding, X., Wang, Z., Rovetta, A. & Zhu, J. Locomotion analysis of hexapod robot. *Proceedings of Conference on Climbing and Walking Robots (CLAWAR)* 291–310 (2010).
32. Steingrube, S., Timme, M., Wörgötter, F. & Manoonpong, P. Self-organized adaptation of a simple neural circuit enables complex robot behaviour. *Nature Physics* **6**, 224–230 (2010).
33. Delcomyn, F. The Locomotion of the Cockroach Periplaneta americana. *Journal of Experimental Biology* **54**, 443–452 (1971).
34. Thrun, S., Burgard, W., Fox, D. *et al. Probabilistic robotics* (MIT press Cambridge, 2005).
35. Dissanayake, M. G., Newman, P., Clark, S., Durrant-Whyte, H. F. & Csorba, M. A solution to the simultaneous localization and map building (slam) problem. *IEEE Transactions on Robotics and Automation* **17**, 229–241 (2001).
36. Tesch, M., Schneider, J. & Choset, H. Using response surfaces and expected improvement to optimize snake robot gait parameters. In *Proceedings of the IEEE/RSJ International Conference on Intelligent Robots and Systems (IROS)*, 1069–1074 (IEEE, 2011).
37. Kober, J., Bagnell, J. A. & Peters, J. Reinforcement learning in robotics: a survey. *The International Journal of Robotics Research* **32**, 1238–1274 (2013).
38. Kohl, N. & Stone, P. Policy gradient reinforcement learning for fast quadrupedal locomotion. In *Proceedings of the IEEE International Conference on Robotics and Automation (ICRA)*, vol. 3, 2619–2624 (IEEE, 2004).
39. Erden, M. S. & Leblebicioğlu, K. Free gait generation with reinforcement learning for a six-legged robot. *Robotics and Autonomous Systems* **56**, 199–212 (2008).
40. Bongard, J., Zykov, V. & Lipson, H. Resilient machines through continuous self-modeling. *Science* **314**, 1118–1121 (2006).
41. Christensen, D. J., Larsen, J. C. & Stoy, K. Fault-tolerant gait learning and morphology optimization of a polymorphic walking robot. *Evolving Systems* **5**, 21–32 (2014).
42. Mahdavi, S. & Bentley, P. Innately adaptive robotics through embodied evolution. *Autonomous Robots* **20**, 149–163 (2006).
43. Koos, S., Cully, A. & Mouret, J.-B. Fast damage recovery in robotics with the t-resilience algorithm. *The International Journal of Robotics Research* **32**, 1700–1723 (2013).
44. Hornby, G., Takamura, S., Yamamoto, T. & Fujita, M. Autonomous evolution of dynamic gaits with two quadruped robots. *IEEE Transactions on Robotics* **21**, 402–410 (2005).
45. Barfoot, T., Earon, E. & D'Eleuterio, G. Experiments in learning distributed control for a hexapod robot. *Robotics and Autonomous Systems* **54**, 864–872 (2006).
46. Koos, S., Mouret, J.-B. & Doncieux, S. The transferability approach: Crossing the reality gap in evolutionary robotics. *IEEE Transactions on Evolutionary Computation* **17**, 122–145 (2013).